Supplementary Information

A strong, tough and cost-effective biodegradable PBAT/lignin composite film *via* intrinsic multiple noncovalent interactions

Shao-Jun Xiong,[a] Si-Jie Zhou,[a] Hao-Hui Wang,[a] Han-Min Wang,[b] Xiao-Jun Shen,[a] Shixin Yu,[*a] Hui Li,[c] Lu Zheng,[d] Jia-Long Wen,[a] Tong-Qi Yuan,[*a] Run-Cang Sun,[e]

[a] Beijing Key Laboratory of Lignocellulosic Chemistry, Beijing Forestry University, Beijing, 100083, China

[b] Tianjin Key Laboratory of pulp and paper, Tianjin University of Science and Technology, Tianjin, 300457, China

[c] Composite Materials & Engineering Center, Washington State University, Pullman, WA, 99164, USA

[d] Jining Mingsheng New Materials Co., Ltd., Jining, 272000, China

[e] Center for Lignocellulosic Chemistry and Biomaterials, Dalian Polytechnic University, Dalian, 116034, China

[*] Corresponding author. Beijing Key Laboratory of Lignocellulosic Chemistry, Beijing Forestry University, Beijing, 100083, China.

E-mail addresses: yushixin@bjfu.edu.cn (S. Yu); ytq581234@bjfu.edu.cn (T.Q. Yuan)

S1: The detailed analysis of the structural characterization of lignin fractions.

Organic solvent fractionation is an efficient method for tuning and improving the homogeneity of the lignin structure. Fig. 2A showed that the M_w of lignin fractions increased with their solubility improvement in the organic solvents (from 1530 g/mol for EL to 4580 g/mol for AL) and the final insoluble fraction possessed the highest M_w (7250 g/mol for RL). The lower PDI value of lignin fractions compared to that of raw kraft lignin suggested that more homogenous lignin was obtained. The high-molecular-weight lignin displayed a higher PDI value, which can be attributed to the presence of the low-molecular-weight lignin fractions [1]. The yield (Fig. S1) of the lignin fractions showed that over half of the lignin was soluble in the organic solvent used. The yield of EL (23.68%) was similar to that of ML (21.37%), while the yield of AL was the lowest (9.38%).

The main functional groups (–OH) in lignin fractions were detected by quantitative ^{31}P-NMR (Fig. S2a) and the results were collected (Fig. 2B, Table S2). It showed that fractionated lignin possessed lower phenolic –OH and total –OH than the raw kraft lignin, while the content of aliphatic –OH and carboxylic group (–COOH) did not display a similar trend. Specifically, EL exhibited the lowest numbers of aliphatic –OH and the highest numbers of phenolic –OH and –COOH compared with ML and AL, which indicated that the oxidization of aliphatic –OH was enhanced when the molecular weight became lower [2]. The lower phenolic –OH contents for ML and AL were mostly due to their lower extent of cleavage of β-*O*-4 linkage, which can be verified by following 2D-HSQC spectra. The signals of β-*O*-4 linkage were observed in KL, ML,

and AL except for EL as presented in Fig. 2C and D, E, and F, and the aromatic regions in 2D-HSQC spectra of the lignin fractions were exhibited in Fig. S3. This pointed out that the degree of breakage of β-O-4 linkage in EL was much higher than that in ML and AL. It can be found that large numbers of β-β linkage are presented in KL, and this result originated from the formation of condensed bonds during kraft pulping. In addition, the weak signal about β-5 linkage was observed in KL, ML, and AL. In addition to the changes in linkages, it was also found that the associated polysaccharide in the fractionated lignin structure was removed after fractionation.

As presented in Fig. 2G, H and Fig. S4A, the maximum degradation temperature (T_{max}) of EL was the highest (403 °C), and this is because it is rich in C-C linkages (β-β and β-5). The lowest T_{max} of ML was presented for the presence of higher content of the β-O-4 linkage that tended to rupture at lower temperatures [3,4], while the T_{max} of AL and RL was similar (Fig. 2G). Additionally, the char content of EL at 600 °C was 34% lower than ML (54%) and AL (52%), which was due to the low molecular weight of EL (Fig. S4B). The char content of RL was highest for its high molecular weight. It can be found that all the fractionated lignin fractions displayed lower T_g than that of KL while the T_g value of RL was the highest one (Fig. 2H). The decreased T_g of EL was primarily due to the decrement of the molecular weight, which provided more free volume for the motion of the lignin macromolecule [5]. The content of the hydroxyl group presented in EL was higher than in ML and AL, which meant that stronger hydrogen bonds existed in EL [6].

Based on the above analysis, the qualitative elucidation of lignin fractions could be established. EL displayed a shorter molecular segment and possessed a more abundant hydroxyl group, and the structure of EL was probably branched rather than linear since its high proportion of β-β linkage. The molecular structure of EL is beneficial in reducing the T_g and steric hindrance, which was favorable to activating the positive effects of the noncovalent interactions and improving the mechanical properties of the lignin-based composite films [2,7]. However, other lignin fractions (ML and AL) may be detrimental to the preparation of composites because their high T_g limited their good melt mixability with PBAT.

S2: The brief techno-economic analysis (TEA) of industrial-scale lignin fractionation using ethyl acetate

Jiang et al. reported a 10-year production line for industrial solvent fractionation of lignin that consumed 150 tons of raw lignin per day [8]. The techno-economic analysis (TEA) revealed that the minimum product selling prices (MPSP) of low molecular weight lignin (LMW) ranged from $726 to $999 per ton depending on the scenario chosen [8].

Herein, the TMA methods and simulation proposed by Jiang et al. were adopted to provide a brief estimate of the price of EL. The financial assumptions of the summary simulation were presented in Table S5. Based on the existing equipment of the pulp mill company, the production line can reach 80% capacity before investment, followed by 100% operation after 50% of the capital expenditure (CAPEX) is invested in

upgrading in the first year of the project, and the remaining 50% is invested in the second year [8].

A typical mass balance of lignin fractionation using ethyl acetate with a 150-ton-per-day capacity is shown in Table S6. The mass balance showed that the loss of solvent was mainly in the dry concentration of soluble components, while the capacity of ethyl acetate lignin was 34.5 ton per day. The capacity of insoluble lignin was 115.5 tons per day and the insoluble lignin was sold at the price of lignin raw materials. The CAPEX for industrial-scale lignin fractionation using ethyl acetate was estimated at 25.4 USD million (Table S7), which is assumed to be the same as the CAPEX for fractionation using ethanol in the work of Jiang et al. [8] since the similar boiling point and solid-liquid ratio. The manufacturing cost of fractionating raw lignin was approximately 594 USD per ton. The estimated minimum product selling prices (MPSP) to achieve a net present value (NPV) of zero at 16% hurdle rates was 1155 USD per ton (Table S7). Based on the TEA, the MPSP of EL has increased significantly compared to that the cost of kraft lignin.

Reference

[1]   Saito T, Brown RH, Hunt MA, Pickel DL, Pickel JM, Messman JM, et al. Turning renewable resources into value-added polymer: development of lignin-based thermoplastic. Green Chem 2012;14(12):3295-303.

[2]   Gioia C, Lo Re G, Lawoko M, Berglund L. Tunable Thermosetting Epoxies Based on Fractionated and Well-Characterized Lignins. J Am Chem Soc 2018;140(11):4054-61.

[3]   Khan MA, Ashraf SM. Studies on thermal characterization of lignin. J Therm Anal Calorim 2007;89(3):993-1000.

[4]   Brebu M, Tamminen T, Spiridon I. Thermal degradation of various lignins by TG-MS/FTIR

and Py-GC-MS. J Anal Appl Pyrolysis 2013;104:531-9.

[5]   Park SY, Kim J-Y, Youn HJ, Choi JW. Fractionation of lignin macromolecules by sequential organic solvents systems and their characterization for further valuable applications. Int J Biol Macromol 2018;106:793-802.

[6]   Kubo S, Kadla JF. Hydrogen bonding in lignin: A Fourier transform infrared model compound study. Biomacromolecules 2005;6(5):2815-21.

[7]   Zhang H, Bai Y, Yu B, Liu X, Chen F. A practicable process for lignin color reduction: fractionation of lignin using methanol/water as a solvent. Green Chem 2017;19(21):5152-62.

[8]   X. Jiang, C. Abbati de Assis, M. Kollman, R. Sun, H. Jameel, H.-m. Chang and R. Gonzalez, Green Chem., 2020, 22, 7448-7459.

Table S1. Composition of the composite films

Sample	Composition (wt%)				
	PBAT	KL	EL	ML	AL
PBAT	100	--	--	--	--
P/KL$_{30}$	70	30	--	--	--
P/EL$_{30}$	70	--	30	--	--
P/ML$_{30}$	70	--	--	30	--
P/AL$_{30}$	70	--	--	--	30
P/EL$_{40}$	60	--	40	--	--
P/EL$_{50}$	50	--	50	--	--
P/EL$_{60}$	40	--	60	--	--
P/EL$_{70}$	30	--	70	--	--

Table S2. The functional groups content and distribution of the lignin fractions

Sample	Aliphatic –OH	Guaiacyl –OH		p-hydroxyphenyl –OH	Phenolic –OH	–COOH[c]	Total –OH
		C[a]	NC[b]				
KL	1.60	2.23	2.46	0.50	5.18	0.89	7.67
EL	1.08	1.79	2.47	0.37	4.63	1.12	6.83
ML	1.66	1.67	1.78	0.40	3.84	0.79	6.29
AL	1.23	1.80	1.72	0.37	3.88	0.46	5.57

[a] Condensed, [b] non-condensed, [c] carboxylic group

Table S3. Tensile properties of lignin/PBAT composite films detected at 25 °C

Sample	Tensile strength (MPa)	Elongation at break (%)	Yield strength (MPa)	Young's modulus (MPa)
PBAT	30.66±2.74	882.70±87.75	3.12±0.11	64.23±3.66
P/KL$_{30}$	10.86±0.51	62.03±6.75	5.39±0.43	175.87±8.54
P/EL$_{30}$	26.68±1.97	780.95±20.91	2.89±0.39	118.79±9.37
P/ML$_{30}$	11.27±1.16	62.49±16.97	5.06±0.23	151.88±13.35
P/AL$_{30}$	11.02±0.44	62.51±14.44	5.28±0.26	162.58±6.56
P/EL$_{40}$	21.81±1.05	814.07±22.84	0.69±0.09	71.44±12.77
P/EL$_{50}$	24.71±2.55	494.73±41.53	9.65±0.26	557.37±23.72

Table S4. DSC results of lignin/PBAT composites

	T_g (°C)	T_m (°C)
PBAT	-37.02	126.11
P/KL$_{30}$	-31.72	125.00
P/EL$_{30}$	-21.89	119.41
P/ML$_{30}$	-30.78	125.46
P/AL$_{30}$	-31.37	127.53
P/EL$_{40}$	-11.11	116.18
P/EL$_{50}$	-8.44	112.70
P/EL$_{60}$	16.40	ND [a]
P/EL$_{70}$	20.46	ND

[a] Not detected

Table S5. Financial assumptions

Input	Unit	Value
Project year 0	% of plant capacity	80%
Project year 1	% of plant capacity	100%
Project life	Years	10
% of CAPEX spent in year-2		50%
% of CAPEX spent in year-1		50%

Table S6. Typical mass balance of industrial-scale lignin fractionation using ethyl acetate (ton day^{-1}, stream numbers refer to supporting information reference [10])

Stream	Description	Lignin	Ethyl acetate	Total
1	Lignin	150.00	–	150.00
2	Fresh solvent [a]	–	7.52	7.52
3	Recovered solvent	–	1345.48	1345.48
4	Slurry to filter [b]	150.00	1353.00	1503.00
5	Solution to evaporator [c]	34.50	1303.57	1338.07
6	Wet filter cake to dryer [d]	115.50	49.43	164.93
7	Insoluble lignin fraction [e]	115.50	0.58	116.08
8	Solvent vapor to condenser	–	48.85	48.85
9	Solvent vapor to condenser	–	1294.94	1294.94
10	Solution to drum dryer [f]	34.50	8.63	43.13
11	Soluble lignin fraction (EL) [e]	34.50	0.17	34.67
12	Solvent vapor to condenser	–	8.80	8.80
13	Solvent losses [h]	–	6.77	6.77

[a] The solvent that needed to be supplemented during fractionation.

[b] The density of ethyl acetate is 0.902g/ml, and the solid-liquid ratio of kraft lignin and ethyl acetate is 1g/10ml.

[c] The yield of soluble lignin fraction (EL) is 23.0%.

[d] The mass ratio of solids and liquids in the filter cake is 1: 0.428.

[e] The mass of the residual solvent is 0.5% of final product.

[f] The solids content of the concentrate is 80 wt%.

[h] The solvent loss mass is 0.5% of the amount of recirculated solvent.

Table S7. The operational expenditure (based on 1-ton raw lignin input), capital expenditure, and minimum product selling price (MPSP) for EL.

Details		Value (USD/t)
Operational expenditure	Raw lignin [a]	150.00
	Ethyl acetate	44.12
	Labor [b]	32.10
	Depreciation [b]	49.30
	Others [b, c]	39.10
	Total	314.62
Capital expenditure (CAPEX)		25400000.00
MPSP		1155.26

[a] Raw lignin is dry cake and the price is adjusted to compensate the cost of drying.

[b] Data is drawn from supporting information reference [10].

[c] Including the smaller expenses of electricity, water, gas etc.

Table S8. Results of detailed cost estimation for producing 1 t film: PBAT, P/EL$_{40}$, and P/EL$_{30}$

Sample	Detailed list		Quantity (t)	Cost (USD/t)	Total cost (USD/t)
PBAT	Raw material	PBAT	1.0	3533.5	4207.3
	Process	Film blowing [a]	1.0	673.8	
P/EL$_{40}$	Raw material	PBAT	0.6	2120.1	3480.5
		EL	0.4	462.0	
	Process	Composites pelleting [b]	1.0	224.6	
		Film blowing	1.0	673.8	
P/EL$_{30}$	Raw material	PBAT	0.7	2473.5	3718.4
		EL	0.3	346.5	
	Process	Composites pelleting	1.0	224.6	
		Film blowing	1.0	673.8	

[a] Cost of the blown film process represents the sum of direct and indirect project expenses (labor, energy consumption, and equipment depreciation).
[b] Pellets were prepared through a granulation process, and the cost represents the sum of direct and indirect project expenses (labor, energy consumption, equipment depreciation, packing, and printing).
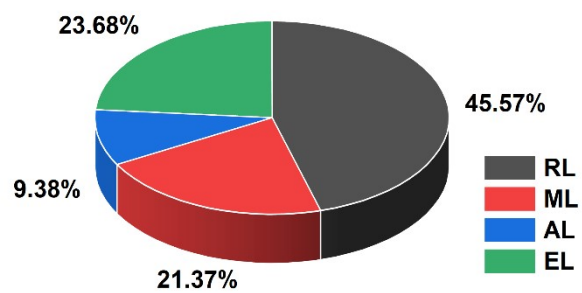
Fig. S1. The yield of the lignin fraction
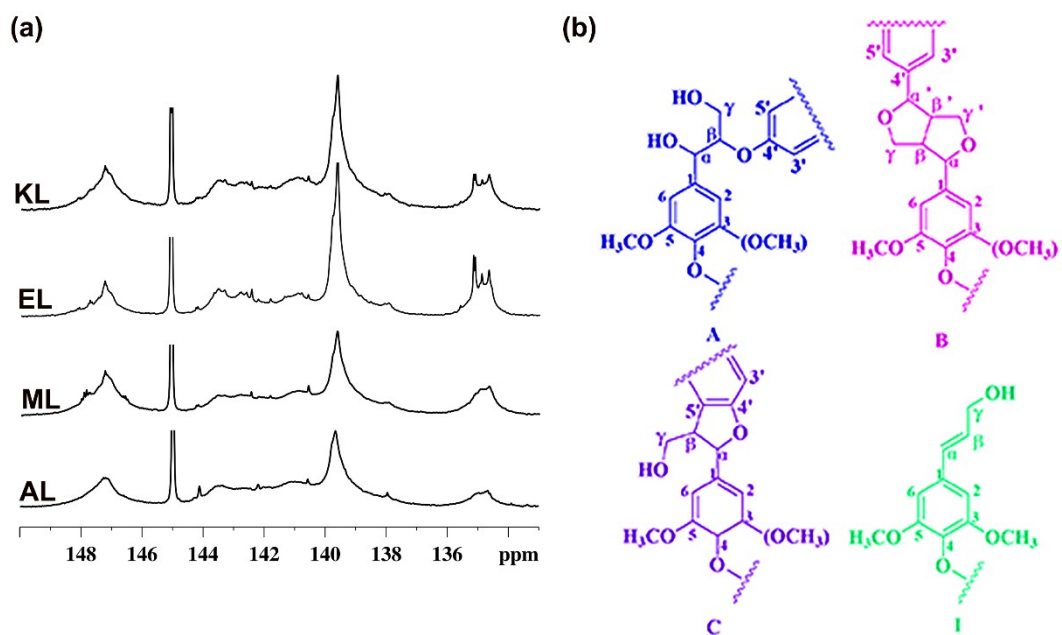
Fig. S2. (a) The quantitative ^{31}P-NMR spectra of lignin fractions and (b) the main side-chain linkages of lignin identified by 2D ^{13}C-^{1}H correlation (HSQC). A) β-aryl ether (β-O-4), B) resinol (β-β), C) phenylcoumaram (β-5), and I) *p*-hydroxycinnamyl alcohol end groups.
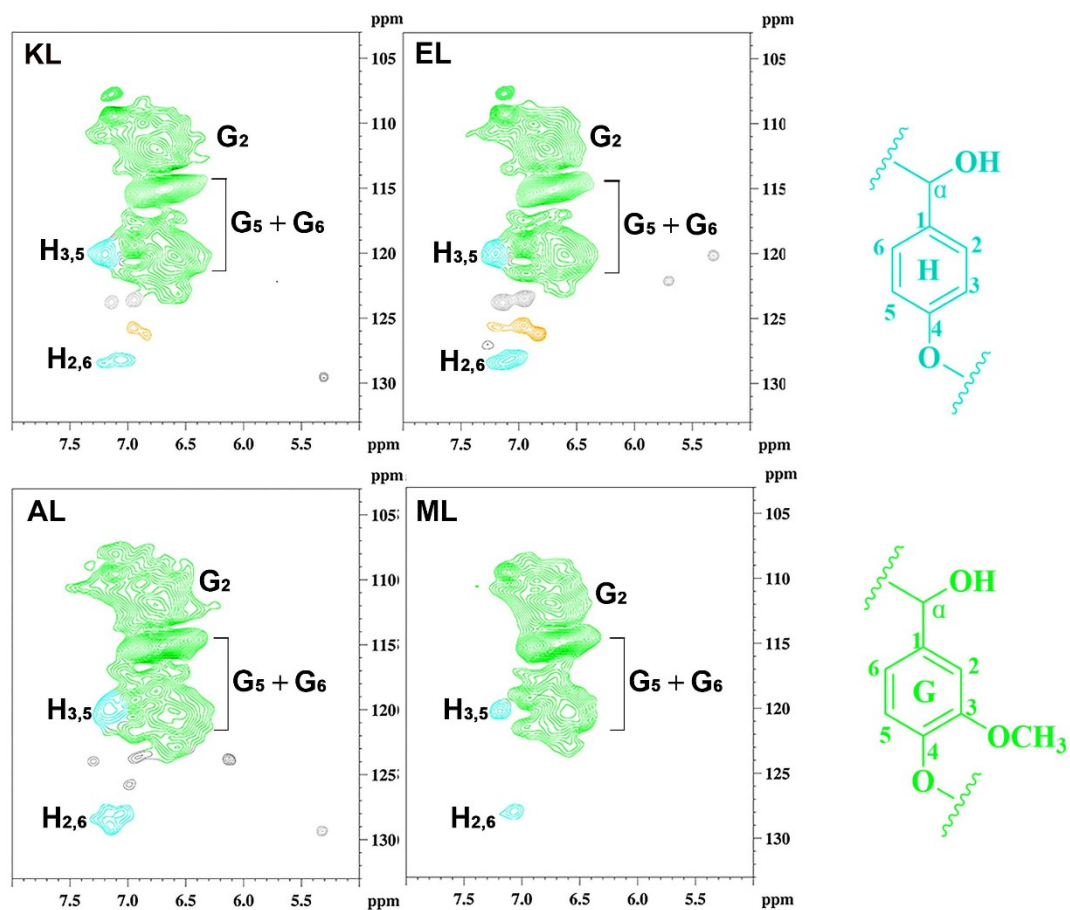
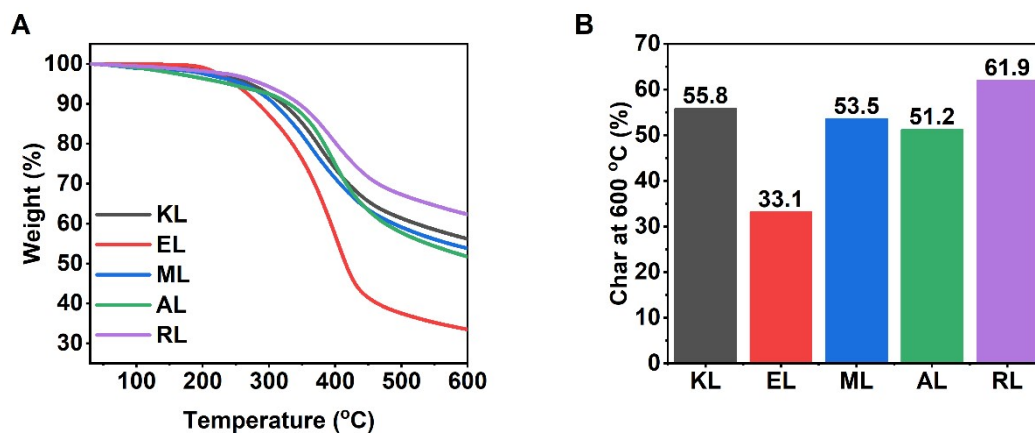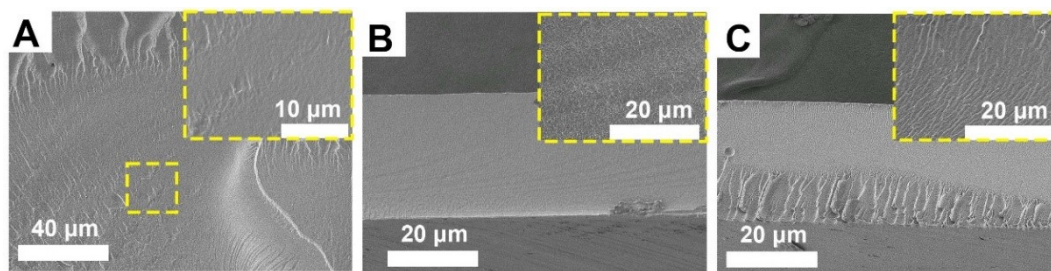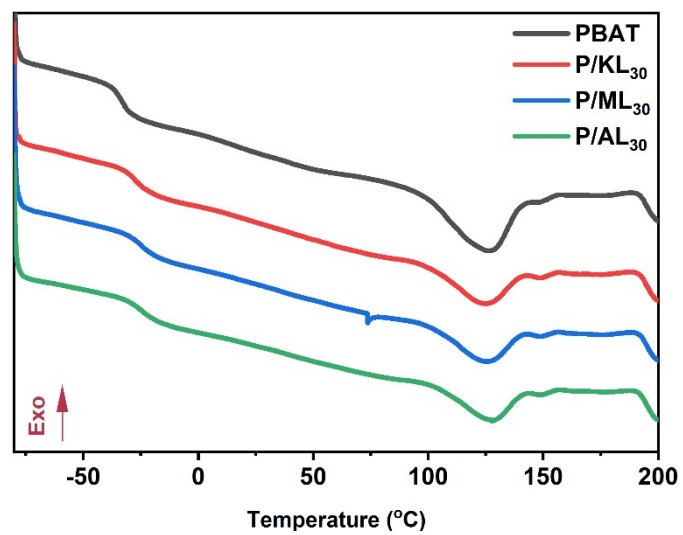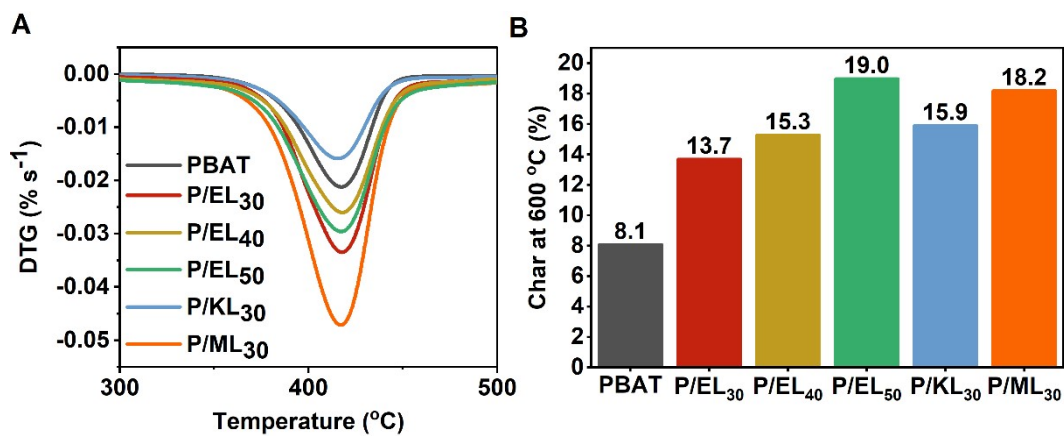**Fig. S3.** The aromatic regions of 2D-HSQC spectra from KL, EL, ML, and AL.

Fig. S4. (A) The TGA curves of KL and its fractions and (B) the char residue at 600 °C of lignin.

Fig. S5. The SEM images of the pure PBAT film and the P/EL composite films. A) PBAT, B) P/EL40, and C) P/EL50. The magnified regions are marked by the yellow squares.
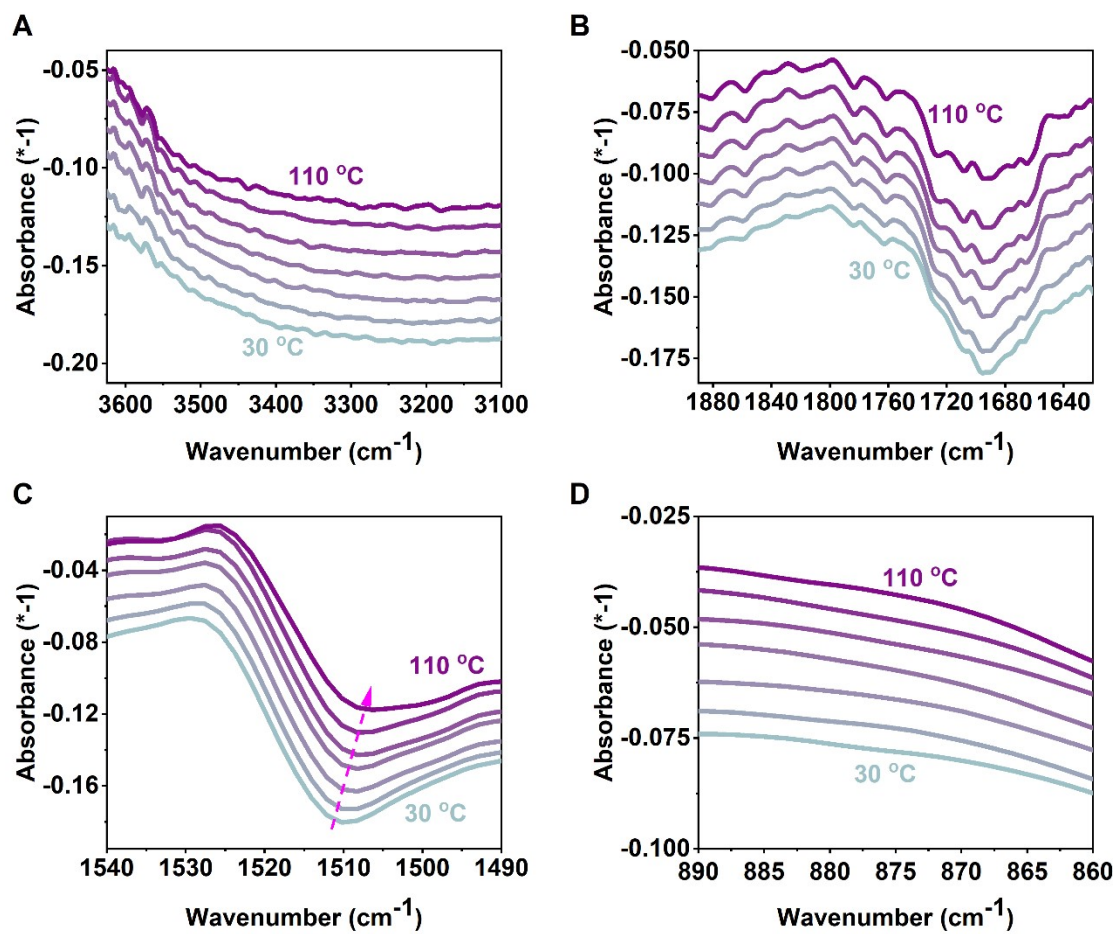
Fig. S6. The DSC curves for PBAT, P/KL$_{30}$, P/ML$_{30}$, and P/AL$_{30}$.
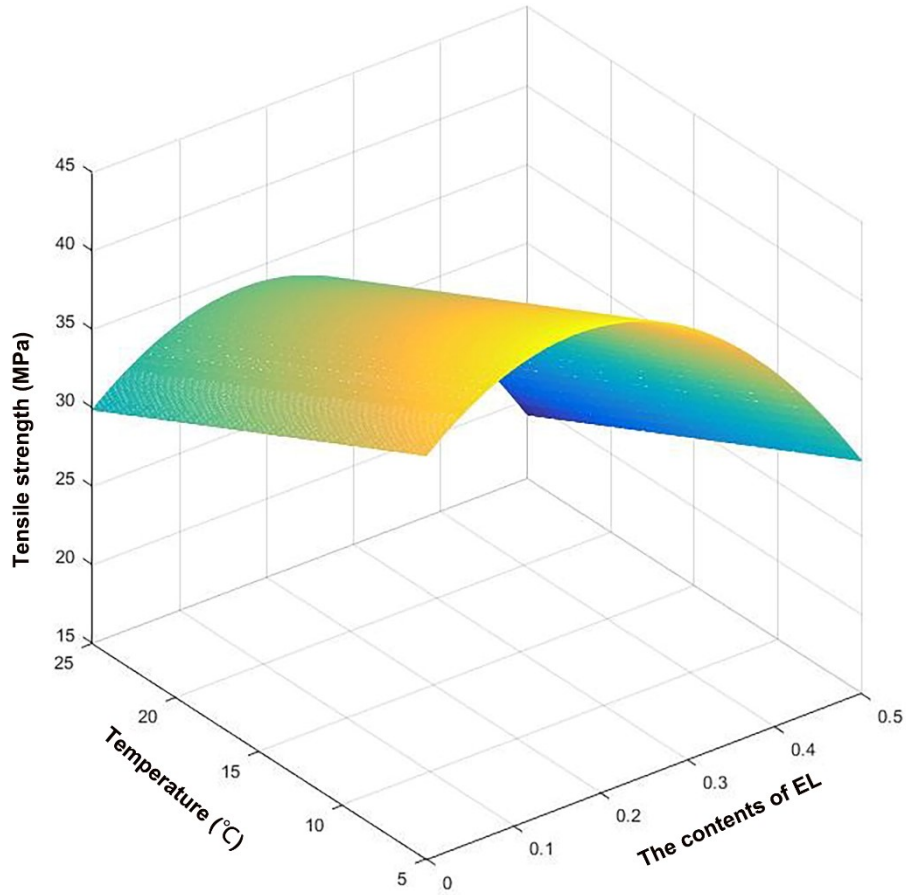
Fig. S7. (A) The DTG curves of PBAT and PBAT/lignin composite films and (B) the char residue at 600 °C of films.
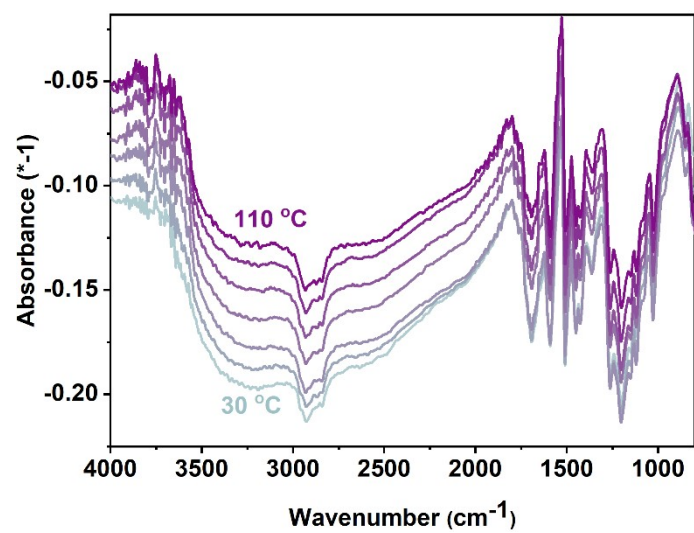
Fig. S8. The temperature-dependent FTIR spectra of EL upon heating from 30 °C to 110 °C (4000–800 cm⁻¹).

Fig. S9. The temperature-dependent FTIR spectra of EL upon heating from 30 °C to 110 °C: A) 3625–3100 cm^{-1}; B) 1890–1620 cm^{-1}; C) 1540–1490 cm^{-1}; D) 890–860 cm^{-1}.

Fig. S10. The three-dimensional fitted images of EL content and temperature versus the tensile strength of the P/EL composite films.
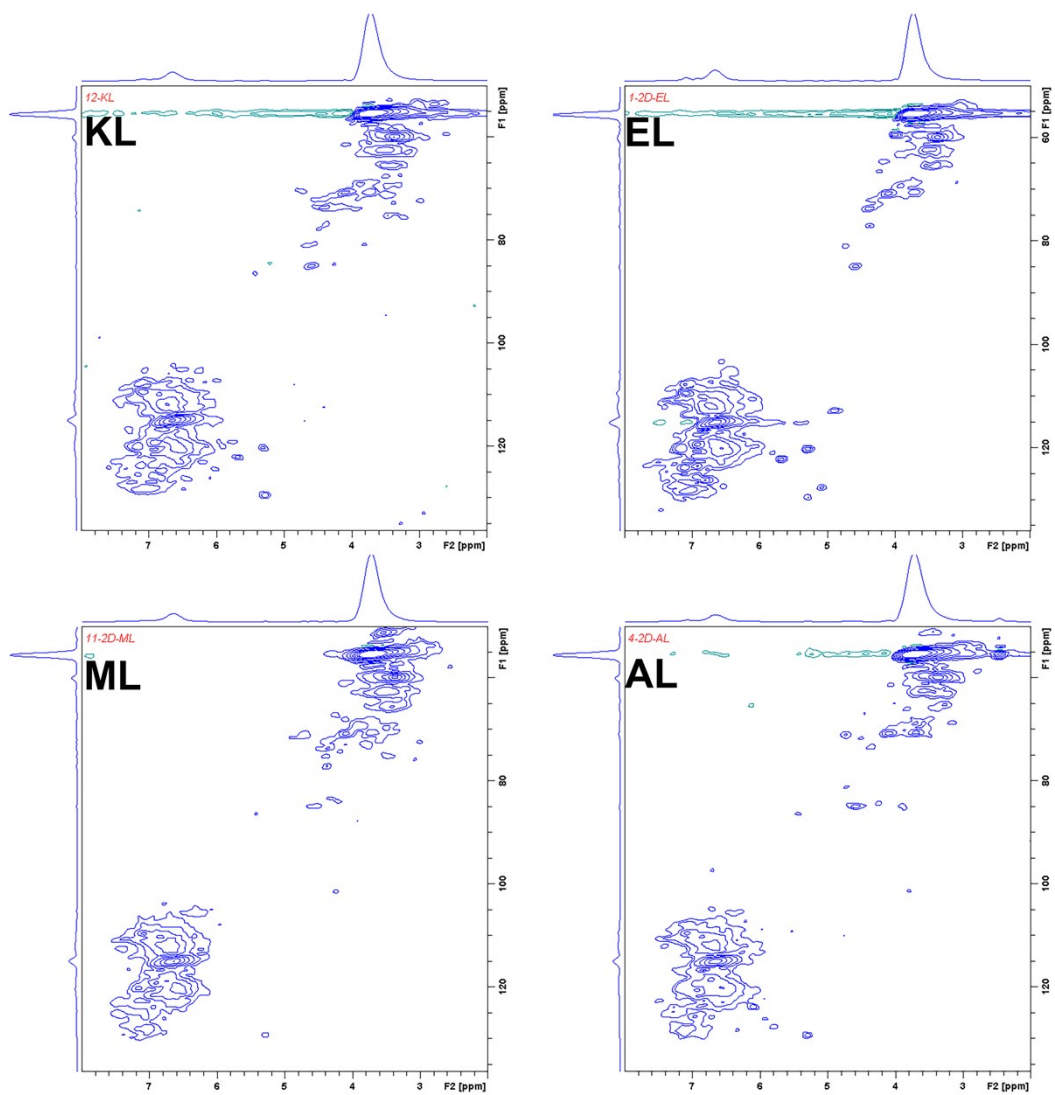
Fig. S11. 2D-HSQC spectra with ^{13}C and ^{1}H NMR plots on x and y-axes from KL, EL, ML, and AL.